coatings

MDPI

Article

Hybrid Organic/Inorganic Piezoelectric Device for Energy Harvesting and Sensing Applications

Mariya Aleksandrova [1,*], Liliya Tudzharska [1], Krasimir Nedelchev [2] and Ivan Kralov [2]

[1] Department of Microelectronics, Technical University of Sofia, 1000 Sofia, Bulgaria
[2] Department of Mechanics, Technical University of Sofia, 1000 Sofia, Bulgaria
* Correspondence: m_aleksandrova@tu-sofia.bg; Tel.: +359-29653085

Abstract: Novel hybrid organic/inorganic flexible devices with composite films, consisting of $Ba_{0.5}Sr_{0.5}TiO_3$ (BST), were prepared by inserting BST nanocoating under spray deposited Polyvinylidene fluoride-based co-polymer PVDF-TrFE. The study validated that the crystalline structure of BST remains unaffected by the presence of polymer. The 3D atomic force microscopic image of the composite sample confirmed the improved surface roughness and contact conditions after spraying the polymer. As a result, the hybrid sample exhibited a higher polarization current with reduced impedance and parasitic inductance. The enhancement of the stability of the piezoelectric parameters at multiple bending was observed for the hybrid sample in comparison with the BST single film transducer. The drop of the root mean square (RMS) voltage was 70% after approximately 340,000 numbers of bending against less than 3% for the hybrid BST+PVDF-TrFE device. Due to the effect of the separate layers and summed net charges, the piezoelectric voltage of the hybrid device was competitive to the piezoelectric oxide films, despite the lower piezoelectric coefficient of the polymer. The proposed solution paves the path toward lead-free, wearable energy harvesting devices for low-power consuming electronic devices.

Keywords: flexible films; hybrid piezoelectrics; nanocoatings; energy harvesting

Citation: Aleksandrova, M.; Tudzharska, L.; Nedelchev, K.; Kralov, I. Hybrid Organic/Inorganic Piezoelectric Device for Energy Harvesting and Sensing Applications. *Coatings* **2023**, *13*, 464. https://doi.org/10.3390/coatings13020464

Academic Editor: Je Moon Yun

Received: 11 January 2023
Revised: 15 February 2023
Accepted: 16 February 2023
Published: 18 February 2023

1. Introduction

Piezoelectric thin-film devices have attracted enormous interest due to their great application prospects towards sensors, energy harvesters, energy storage systems, etc. [1–3]. Piezoelectric oxides with perovskite structure have been widely investigated due to their high piezoelectric coefficients d_{ij} and electromechanical coupling k to know the dependence of the piezoelectric properties and their microstructures and ordering degrees [4,5]. Without a doubt, the most popular representative of piezoelectric oxides is the lead-zirconium titanate (PZT), which exhibits the strongest piezoelectric response, but its application is limited due to the lead contained in the chemical composition. PZT nanostructures have been involved in flexible structures, generating a piezoelectric voltage of up to 8 V, when subjected to force up to 10 N and producing a power density of ~6 $\mu W/cm^2$ at an external load of 1 MΩ [6]. Alternatively, the PZT has been replaced by lead-free piezoelectric oxides, such as $(Na,K)NbO_3$, and they have been combined with polymers such as poly(3-hydroxy butyrate) (PHB) and polyaniline (PANI) to hybridize the device, reinforce their mechanical stability, and increase their conductivity [7]. Mechanical durability is crucial for current wearable devices, which are fabricated onto flexible substrates and attached to the human body for tracking their motion and producing electrical signals proportional to the intensity of the applied loading. ZnO, AlN, and $LiNbO_3$ have been also reported as suitable to replace PZT [8–10]. Wlazło et al. [11] reported an approach for the patterning of ZnO in the nanoscale, using chemical bath synthesis, and investigated the effect of the substrate. As a result, ZnO nanorods with high uniformity and uniaxial alignment were produced. The nanoformations are characterized by enhanced piezoelectric properties, due to the

increased equivalent effective area and single-directional alignment of the dipoles, for which the degree of alignment is substrate-dependent. Similar results have been achieved in [12], where highly efficient ZnO nanowires were produced by the hydrothermal method. Exotic biomaterials, such as bacterial-based cellulose, fish skin, and spider silk, have been also found responsive to vibrations, direct force, or impact, and demonstrated potential applicability for energy harvesting devices [13].

On the other hand, polymer-based piezoelectric materials, such as poly-(vinylidene fluoride) PVDF or its copolymer poly-(vinylidene fluoride) trifluoroethylene (PVDF-TrFE), have several unique advantages over the inorganic materials, such as good mechanical flexibility, chemical stability, biocompatibility [14], and ease of film deposition and processing, such as spin-coating, electrospinning, and spray deposition [15–18]. This non-biodegradable piezoelectric polymer scaffold is a promising core material for manipulating piezoelectric films' behavior. PVDF-TrFE fibers have been usually produced by an electrospinning process. Their higher mechanical strength results in a stronger interconnected fiber network that can maintain its structural integrity during compression and expansion. However, their piezoelectric coefficients and electromechanical coupling are several times weaker than the same factors are with the piezoelectric oxides. Recently, researchers have attempted to improve the piezoelectric properties of this polymer without compromising its mechanical strength or flexibility by incorporating various nucleating agents (nanofillers) into the polymer matrix. Studies have shown that polymer crystallization behavior depends on specific surface interactions between the nucleating agents and polymer chains. The nucleation effect of the nanofillers depends on the particle surface charge and surface area, concentration, dispersion, lattice matching, and processing conditions. The presence of nanofillers has been shown to reduce the energy barrier of nucleation increasing the rate of crystallization and the degree of crystallinity of the polymer for enhancing its piezoelectric response [19].

The hybridization of organic and inorganic piezoelectric materials is a suitable approach for combining their properties. Another aspect of the hybridization is the possibility to combine the effect of polarized charges from the piezoelectric material and the surface charge due to triboelectric effect at mechanical loading [20,21]. This coupling results in a higher efficiency due to the superposition of the charge density and polarized current. One of the impressive works regarding inorganic/organic composite was reported in [22], where $BaTiO_3$ nanopowder and polymer PDMS were in composite relation and, additionally, the co-incorporation of $Ti_{0.8}O_2$ nanosheets was realized together with Ag nanoparticles into the flexible PDMS composite. The fillers boost the electrical response of the hybrid device and maximize its outputs voltage to ~150 V. ZnO nanoparticles have been incorporated into PVDF electrospun nanofibers under high voltage, which essentially aligned the electric dipoles present in the PVDF solution. The degree of alignment is proportional to the magnitude of the applied electric field [23]. The output voltage and current of 0.8 V and 30 nA, respectively, were reported in response to 45° fold and release motion of the human finger motion. Multilayer thick structures of the same materials have generated voltages of 1.75, 1.29, and 0.98 V when an input force of 4 N (2 Hz) was applied at an angle of 0°, 45°, and 90°, respectively. The corresponding measured maximum output power values were 0.064, 0.026, and 0.02 μW, respectively. Furthermore, the prototype generated a stable voltage output for 14,000 bending cycles and successfully converted the strain energy produced by multidirectional input forces from various human movements [24].

Barium titanate (BT) and its solid solutions is a well-known dielectric ceramic with moderate piezoelectric coefficients (d_{33} of 90 and 190 pC/N along the [001] and [111] directions) of the perovskite crystal. BT is promising nucleating filler for PVDF-based composites due to its easy preparation through technologies that allow precise control of its chemical composition [25]. The incorporation of highly crystalline $BaTi_{(1-x)}Zr_xO_3$ (BTZO) nanocubes with sizes around 200 nm in PVDF were shown to provide high electrical parameters of up to ~11.9 V and ~1.35 μA in response to a 21 Hz cycling bending with a constant load of 11 N. In comparison, BT/PVDF film showed output parameters of 7.99 V

and 1.01 µA under the same load conditions [26]. The energy harvesting performance of a PVDF-TrFE matrix-based nanocomposite filled with perovskite potassium sodium niobate (KNN) nanoparticles ranging in size from 30 to 105 nm has also been investigated. The surface modification and volume fraction of KNN are considered to be the critical parameters responsible for the high performance of NG. An output voltage of 0.98 V and an output current of 78 nA were obtained using nanofibers containing 10 vol% KNN [27]. Nunes-Pereira et al. performed comparative studies of the piezoelectric properties of electrospun PVDF-TrFE containing BT nanoparticles of different sizes, specifically 10 nm (cubic), 100 nm (cubic), and 500 nm (tetragonal) particles. Electrospun composite fibers have been compared with pure PVDF fibers. The obtained results showed that the size and content of the filler and its crystal structure determined the piezoelectric properties of the nanocomposites. The authors reported that the increased mechanical stiffness of the composites with larger sizes and nanofiller content reduced the energy harvesting efficiency of the samples, probably due to induced defects [28]. The defects induced by the nanofiller in the polymer matrix can act as vibration absorbers and, therefore, can suppress the conversion of mechanical energy to electrical energy. Furthermore, the random orientation of the domains in the inorganic electroactive filler can lead to an overall decrease in the piezoelectric polarization of the composite, as compared to that of the pure polymer. Thus, although a great amount of research has been carried out using these materials, there are still some limitations related to the agglomeration and phase separation of BT, KN, and similar fillers in the polymer matrix, which cause poor surface interactions and high defect density. Furthermore, the dielectric constant of BT and ZnO particles is unstable at elevated temperatures, which may affect the performance of the composites. As well as the material synthesis, the design of the energy harvesting elements is also significant for the performance of the piezoelectric devices [29].

The fabrication of wearable thin-film energy harvesting or sensing devices based on polymer composites still presents a problem, such as a complex fabrication process, poor reproducibility, small and unstable power output, low economic efficiency, and difficulty in controlling the interface between the inorganic nanostructures and the polymer matrix. The development of simple and low-cost approaches to improve the electrical power output of polymer-based energy converters without forming complex composite structures would be promising for the fabrication of various self-powered and sensing device applications.

In this paper, $Ba_{0.5}Sr_{0.5}TiO_3$ perovskite piezoelectric oxide with stable dielectric permittivity, piezoelectric coefficient, and electromechanical coupling over a broad temperature range was hybridized with the ferroelectric polymer PVDF-TrFE, grown by spray deposition technique for a flexible, thin-film energy conversion device. The study aimed to develop a simple bi-material system involving a hybrid layer of piezoelectric oxide and piezoelectric polymer, and to investigate the samples in terms of energy harvesting ability and mechanical stability. The hybrid device showed very good energy harvesting ability and excellent stability of the piezoelectric response at multiple bending. As a result, the developed flexible composite with an enhanced piezoelectric response and improved mechanical stability has enormous potential for next-generation devices, especially for low-power energy harvesters, sensors, and storage systems applications.

2. Materials and Methods

The substrates were cut from poly(ethylene 2,6-naphthalate) (PEN, Goodfellow, Huntingdon, UK) sheet with a thickness of 465 µm, each piece with size 3 cm × 3 cm, and cleaned in a supersonic bath with a moderately concentrated alkaline solution. The choice of this material was based on its high-temperature resistance, mechanical strength, high adhesive strength of most coatings to its surface, and relatively low cost. The bottom electrode film of aluminum with a thickness of 45 nm was deposited by vacuum thermal evaporation at base pressure 8×10^{-6} Torr with a deposition rate of 150 Å/s from aluminum wire with a purity of 99.998% (Kurt J. Lesker, East Sussex, UK). For patterning the bottom and top square electrode and locating the active zones of 1.5 cm × 1.5 cm, standard photolithography was

used by applying photoresist ma-P 1215 (positive tone, Microresist, Berlin, Germany) and processing the photosensitive coatings according to the manufacturer's recommendations in terms of soft backing, exposure, development, and hard backing [30]. The aluminum films were etched in chemical solution HNO_3:HCl:H_2O mixed in a ratio 1:1:1.

The first layer of piezoelectric polymer was spray deposited at 70 °C by a semi-automated spray coater with a fine nozzle (2 μm orifice) under the pressure of 3.5 bar. The solution was prepared to be pulverized from PVDF-TrFE (Sigma Aldrich–Merck, Darmstadt, Germany) dissolved in methyl ethyl ketone (purity 99.9%, Valerus, Sofia, Bulgaria) solvent with a concentration of 4 mg/mL and after stirring for 1 h at 40 °C, the solution was sprayed for 24 s with 3 s durations of the spray pulses and 5 s durations of the pauses in between. The pauses were set to provide sufficient time for the evaporation of the solvent and ensure uniform distribution of the delivered aerosols without solution leaking. The film thickness was 440 nm.

The deposition of the piezoelectric oxide film from barium strontium titanate $Ba_{x-1}Sr_xTiO_3$ (BST) was carried out by vacuum reactive radiofrequency sputtering of a 3-inch target (purity 99.9%, (Kurt J. Lesker, East Sussex, UK) at a plasma current of 130 mA and a sputtering voltage of 600 V. The oxygen partial pressure was 1×10^{-3} Torr (introduced at a base pressure of 1×10^{-6} Torr) and the sputtering argon gas pressure was set to 1×10^{-2} Torr. The film thickness was 375 nm. The deposition conditions selection was connected with the obtainment of specific chemical composition of the solid solution of BST, for which the piezoelectric response was the strongest. Details about the confirmation of the chemical composition of the BST by FTIR and XPS, as well as a study of the surface morphology by SEM, can be found in a previous study [31]. Then, the spray deposition process was repeated to produce a second film from PVDF-TrFE, covering the BST. In the end, top aluminum film was grown and patterned following the same technology flow as for the bottom electrode.

The crystalline structure was investigated using Philips PW-1724 (Amsterdam, The Netherlands) X-ray diffraction (XRD) patterns with CuKα radiation. Then, 3D topographies of the film surfaces were scanned by atomic force microscope (AFM) MFP-3D, Asylum Research, Oxford Instruments (Abingdon, UK) in non-contact mode. To investigate the quality of contact at the films' interfaces, electrical impedance spectroscopy was applied, by impedance analyzer Hioki IM3590 (Nagano, Japan). The basic accuracy of the device for the impedance component measurements was Z: $\pm 0.05\%$ and θ: $\pm 0.03^{\circ}$. To investigate the ability for conversion of force into electrical charges, the devices were measured by d_{33}-meter PolyK Technologies PK-D3-F10N (Philipsburg, PA, USA) in the force range from zero up to 10 N. The measurement error for the piezoelectric module estimation was $\leq \pm 2\%$. For the dynamic testing of the samples and evaluation of the durability at multiple bending, a homemade electromechanical setup was used with variable intensity and frequency of vibration, causing a variety of possible deflection positions of the cantilever, and different bending degrees of the samples. The alternative voltage and current were measured by Agilent B2985A electrometer (Santa Clara, CA, USA) with 6.5 digits resolution. The oscillograms were observed on the digital storage oscilloscope Tektronix TDS 1012B (Beaverton, OR, USA). All measurements were conducted with no electric load (open circuit mode) at room temperature. For comparison, results from the electrical characterization of a simple single-layer BST-based energy harvesting devices were given. For the electrical measurements, an array of 5 samples were prepared, patterned according to the presented topology in Figure 1a, and measured. The active layers were situated between the set of two combs of the electrode network. For the AFM, three points randomly selected from the area under study were scanned and one of them showed.

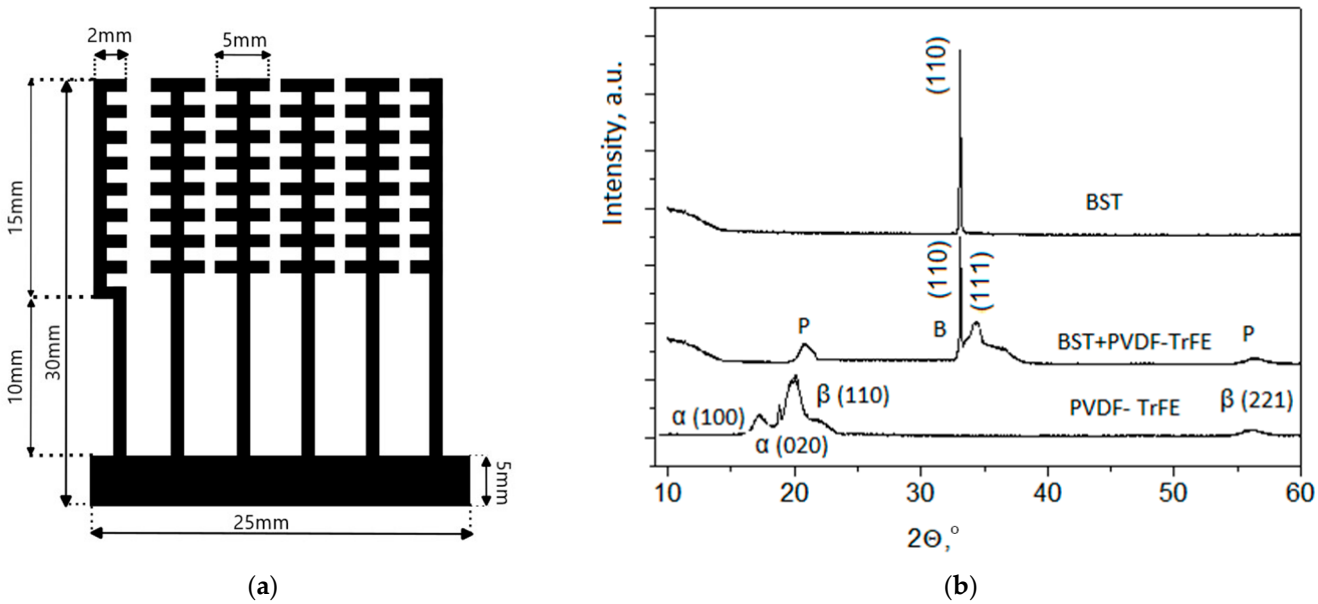

(**a**) (**b**)

Figure 1. Design of the measured sample (**a**) and XRD patterns of BST, PVDF-TrFE, and BST+PVDF-TrFE composite (**b**).

3. Results and Discussion

According to the XRD measurement, shown in Figure 1, a crystalline film was obtained at these deposition conditions having perovskite structure as was indicated by the presence of a strong peak at $2\theta = 33°$ [31]. The PVDF-TrFE sample shows the mixture of α and β phases. The most intense (110) and weak (221) peaks in the diffractogram corresponded to β phase and the other two were associated with α phase [32]. The XRD patterns of the BST+PVDF-TrFE-based composite sample indicated the presence of all the diffraction peaks of the BST phase, whereas the intensity of peaks corresponding to PVDF-TrFE were suppressed, probably due to the semi-crystalline nature of the polymer. BST is a pure crystalline solid solution, thus the crystalline contribution from BST was stronger and influenced with stronger signal in the resulting composite over the corresponding P(VDF-HFP) peaks, which remained weaker. The features of PVDF-TrFE in the composite XRD curve were marked with P and the features of BST–with B. It can be noted that there was no shift in (110) peak for the composite, as compared to the pure BST, which is sufficient proof that the BST structure was retained in the composite and it remained unaltered by the presence of the piezoelectric polymer. Therefore, there was no significant structural modulation of BST after its combining with the PVDF-TrFE layers, except the appeared additional (111) peak, which, however, cannot be ascribed to the presence of the polymer. The origin of this peak should be additionally explored, but at this stage, it can be suggested that it appeared after the heating of the already-grown film during the deposition of the second polymeric layer. Thus, the samples fulfilled the condition for a hybrid organic/inorganic structure with an interface between the films.

According to the Scherrer Equation (1), the nano crystallite size (L) can be calculated by taking into account the wavelength λ (nm) of the XRD radiation, the full width at half maximum of peaks (β) and radian angle 2θ in the pattern [33]. There is a shape factor K which is usually accepted as 0.94.

$$L = \frac{K\lambda}{\beta \cos\theta} \quad (1)$$

The average size of the hybrid BST+PVDF-TrFE was found to be 24 nm, which was smaller as compared to the BST only, where 33.5 nm was calculated for the crystallite size. The addition of filler to PE lead to a slight decrease in the crystallite size.

The next step was to characterize the fabricated hybrid elements by evaluating the quality of the contacts, the measurement of the piezoelectric coefficient, and investigating

the long-term stability in dynamic mode and resonance conditions. The measurements were conducted for pure BST and composite BST+PVDF-TrFE devices on PVDF-TrFE-coated PEN substrate.

The contacts quality was estimated by impedance measurement in two different modes–impedance and phase shift between the current and the voltage over the sample (Z-θ) against frequency (Bode plot), as well as serial capacitance and contact resistance (C_s-R_s), extracted from the RC equivalent electrical circuit, against frequency (Table 1, Figures 2 and 3).

Table 1. Comparison of the main parameters measured by impedance spectroscopy for the pure BST and hybrid PVDF-TrFE/BST/PVDF-TrFE samples.

Sample Type	Z, kΩ	θ, °	C_s, F	R_s, Ω
BST	237.48	−88.58	3.26×10^{-12}	6.04×10^{3}
BST+PVDF-TrFE	2.37	−5.62	31.3×10^{-9}	848.92

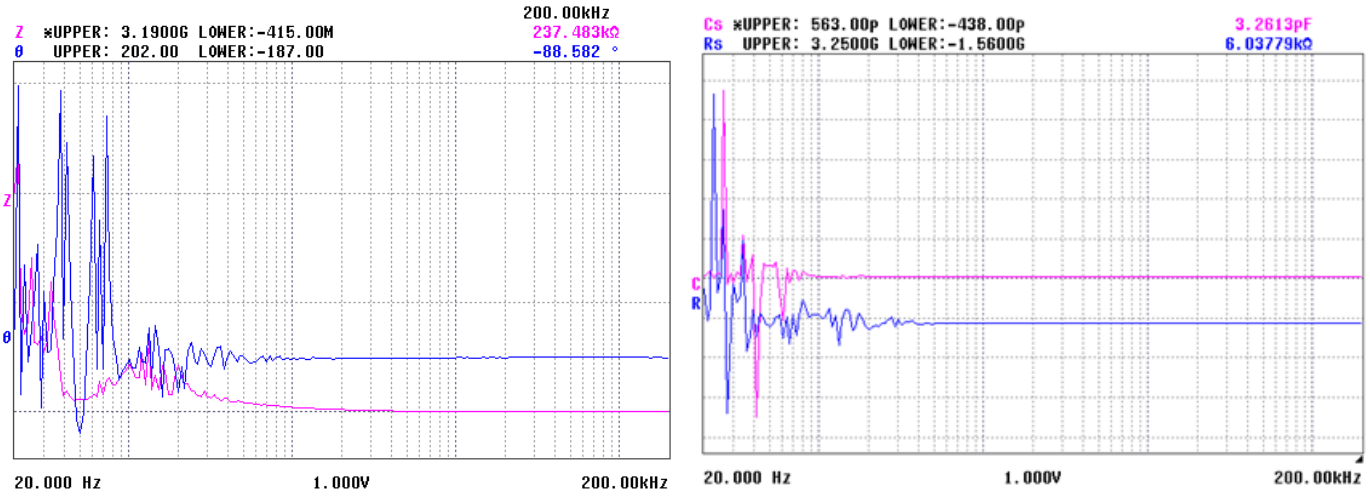

(**a**) (**b**)

Figure 2. Bode plot (**a**) and frequency sweep of the contact parameters (**b**) of BST sample.

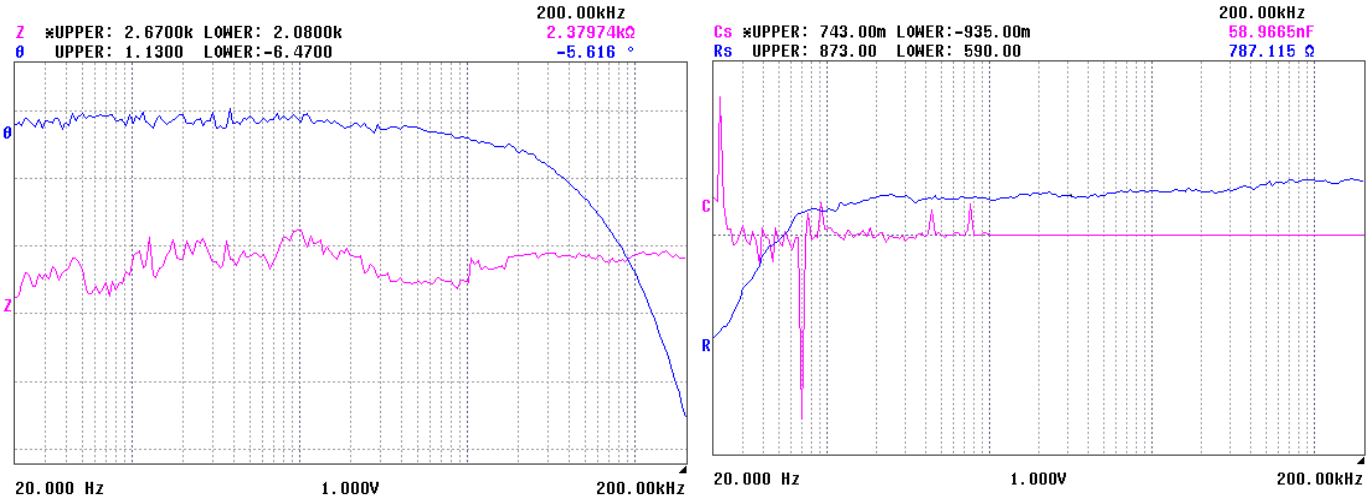

(**a**) (**b**)

Figure 3. Bode plot (**a**) and frequency sweep of the contact parameters (**b**) of PVDF-TrFE/BST/PVDF-TrFE sample.

Comparing the two samples, it can be seen that the capacitance of the non-hybrid BST device (Figure 2b) was four orders of magnitude lower than the value measured for the PVDF-TrFE/BST/PVDF-TrFE sample (Figure 3b). The latter was a sum of the contributing capacitances of the two materials [34]. The contact resistance was two orders of magnitude lower for the hybrid device (Figure 3b), as compared to the single BST device (Figure 2b), which was due to the lower surface roughness of the multilayer stack and the contacting surfaces to the electrodes. This hypothesis was further confirmed by the AFM study of the BST on PEN, BST on PVDF-TrFE-coated PEN, and the PVDF-TrFE film on BST/PVDF-TrFE/PEN, shown, respectively, in Figure 4a–c.

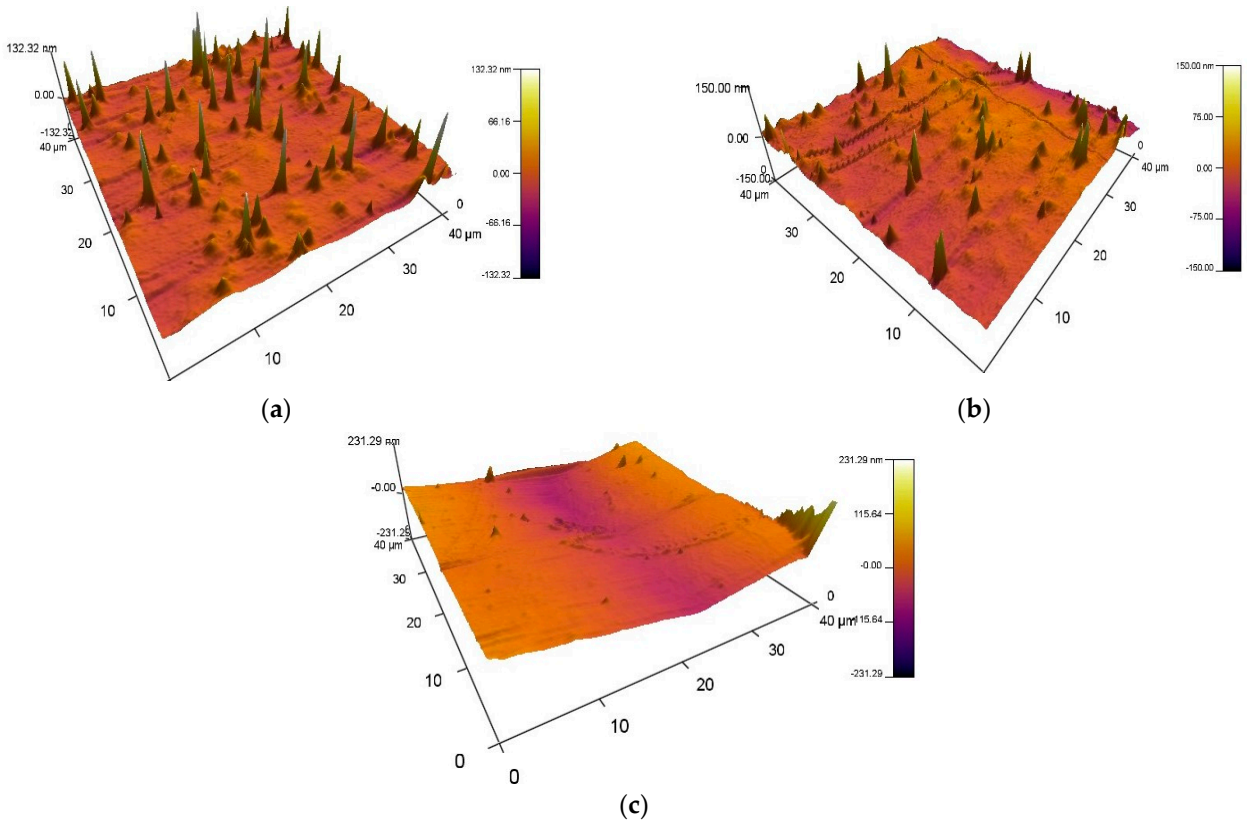

Figure 4. AFM 3D study of the surface topography of the different coatings grown on PEN substrate: BST film (**a**); BST film of PVDF-TrFE-coated PEN (**b**) and PVDF-TrFE film on BST/PVDF-TrFE/PEN (**c**).

The AFM data showed that the RMS roughness of BST film only was 15.5 nm, for BST grown on the semi-crystalline polymer, the effective roughness was lower and approximately 12.2 nm, and for the multilayer stack of PVDF-TrFE/BST/PVDF-TrFE/PEN, the scanned top surface showed the lowest RMS roughness of 9.6 nm. Thus, the contact area for the hybrid device was the greatest, which can explain the lower contact resistance.

The low capacitance of ~3.2 pF (Figure 2a) can be ascribed to partial dielectric relaxation of polarization charges and, thus, significant enhancement of the piezoelectricity should not be expected in contrast to the multilayer hybrid sample. Furthermore, the Bode plot showed two orders of magnitude higher impedance of ~237.4 kΩ for the single layer device (Figure 2a), which is an indication of higher voltage drop over the piezoelectric element at open circuit and, therefore, can serve as a voltage source only, without having the ability to produce sufficient current for power harvesting function [35]. The value of the phase shift angle of −88° shows dominant inductive character of the BST-based element, which can be ascribed to the parasitic inductance of the contacts due to the sharp formations in the film topology and the unstable point contact between the functional film and the electrode layer. On the contrary, the impedance of the composite device was found to be ~2.3 kΩ, which meant a better ability to provide current flow when a load was attached.

In addition, the Theta value of −5° showed that the overall behavior of the element was away from inductance, which further confirms that the polymer introduction resulted in smooth surfaces in contact with the electrodes, leading to improved interface conditions of the piezoelectric hybrid transducer. These results are proof that the introduction of a composite between the piezoelectric oxide and polymer is an efficient approach to improve the contact conditions of the system, which is a prerequisite for enhanced piezoelectricity and optimized power output.

The measurement of the piezoelectric coefficient d_{33} together with the internal force experienced from the sample are presented and compared in Figure 5a,b for applied external force varying between 1 and 10 N with a frequency of the shaker tool of 110 Hz.

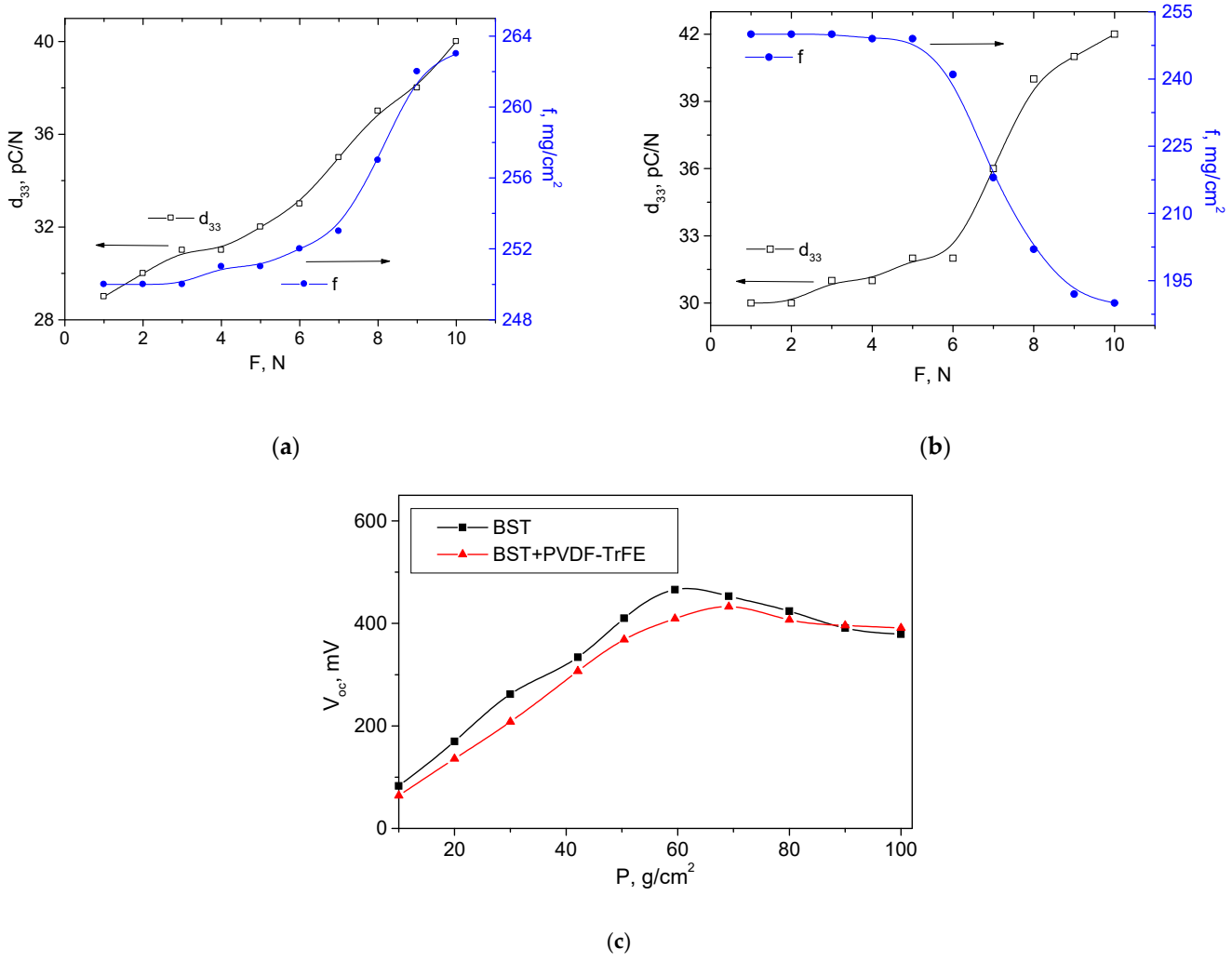

Figure 5. Piezoelectric coefficient and internal force for BST single material sample (**a**) hybrid BST+PVDF-TrFE multilayer device (**b**), and open circuit voltage versus pressure at a resonant frequency for the two devices (**c**).

As can be seen in Figure 5a, by increasing the external force over the BST-based device, the internal forces almost exponentially increased from 250 to 263 mg/cm^2. As a consequence, the piezoelectric coefficient also slightly increased from 29 to 40 pC/N, following a similar trend of rising, similar to the internal force. The results, however, showed untypical behavior of the internal force experienced from the hybrid device, although the curve of the d_{33} remained similar, as compared to the single layer device, as is visible from Figure 5b. A reason for this could be that the polymer layer (PVDF-TrFE) absorbs the mechanical waves, which in turn do not fully reach the next piezoelectric layer consisting of BST. Another possibility is anisotropy in the PVDF-TrFE-sprayed layer, whose response was

weaker when force was applied in the vertical direction and the charge was measured in the same direction compared to a case where the vibration propagated horizontally, i.e., the coefficient d_{31} could possibly be greater than d_{33}. This will be clarified at a later stage during the dynamic test, where, if this hypothesis is not true, the sample will not exhibit a strong piezoelectric response at resonance. The sensitivity of the two kinds of transducers was similar, considering the dynamic range of the piezoelectric coefficient at constant force applied. A plot of open circuit voltage versus pressure at a resonant frequency for the BST only and hybrid BST+ PVDF-TrFE multilayer device was shown in Figure 5c. As is seen, the hybrid device exhibited a gradual increase in the output voltage and at loading near 70 g/cm^2, the voltage remained stable, showing small variation and negligible decrease in the voltage. This limit of the response can be ascribed to the small thickness of the film, resulting in relatively fast orientation of the dipoles, after which the piezoelectric effect decayed due to large strain induced in the lattice and depolarization fields [36]. In contrast, the BST single material sample showed its maximal output voltage (although higher than the voltage of the hybrid device) at a lower loading of ~60 g/cm^2 and a consequent gradual decrease in the voltage with a rate 525 μV/g. This effect can be ascribed to defects in the lattice and structure degradation due to the brittleness of barium strontium titanate. This is a proof for the contribution of the PVDF-TrFE materials to the durability and reliability of the energy harvester.

The next step of the device characterization was the dynamic testing for durability at mechanical loading and degradation evaluation. The lab-made setup was pre-calibrated with reference strain gauges to find the correlation between the electrical signal supplied by the generator and the strength of the induced vibration. According to the geometric dimensions and shape of the tip (trapezoidal), it is known in advance at what signal amplitude, what deviation of the tip (respectively of the sample) is caused, and what mass load corresponds to it. For this purpose, the samples must have a rectangular shape and be joined symmetrically to a central point of their short side. With the oscilloscope and the electrometer, the shape and the effective values of the piezoelectric alternative voltage and current were monitored. The attenuation of the signal was tracked at the beginning of the measurement, after one hour and after two hours. The resonance frequencies of the samples were 48 Hz and 42 Hz for the single BST device and hybrid device, respectively. Therefore, the single material device was subjected to 172,800 bending cycles for an hour and 345,600 for two hours. Similarly, for the hybrid device to be valid, one hour of bending was equivalent to 151,200 bending cycles for an hour and 302,400 bending cycles for two hours. Figure 6a–f shows the shape of the output voltages of the two kinds of samples immediately at switching on, after 1 h of bending and after 2 h of bending. Additionally, the short circuit current through the samples was measured and the values were summarized in Table 2, together with the effective voltage and power produced without load. The small values of the quantities can be explained by the small active area of the prepared samples, the small thickness of the functional films, and the relatively low applied force. As can be seen in Figure 6a–c, the shape of the sinusoidal signal was more regular and the sinusoids are smoother without harmonic distortion due to the piezoelectric oxide, which was characterized by a well-established, strong piezoelectric response, because of the strictly defined periodicity of the crystal lattice of the piezoelectric ceramic materials, compared to the piezoelectric polymers. The peaks of the output voltage for the hybrid device (Figure 6d–f) looked modulated, due to the combined, overlapped contribution of the separate films to the overall sum of piezoelectric charges. Regardless, it is clear that the stability of the signal against the time was more stable in this case. In summary, the signal from the BST samples varied with an average 1 V after 2 h of constant bending, while the hybrid device kept the signal stable in magnitude for the same duration and parameters of cyclic loading. Signals overlapping could be observed for the hybrid material, but they were not classified as distortions, as was the case with BST only.

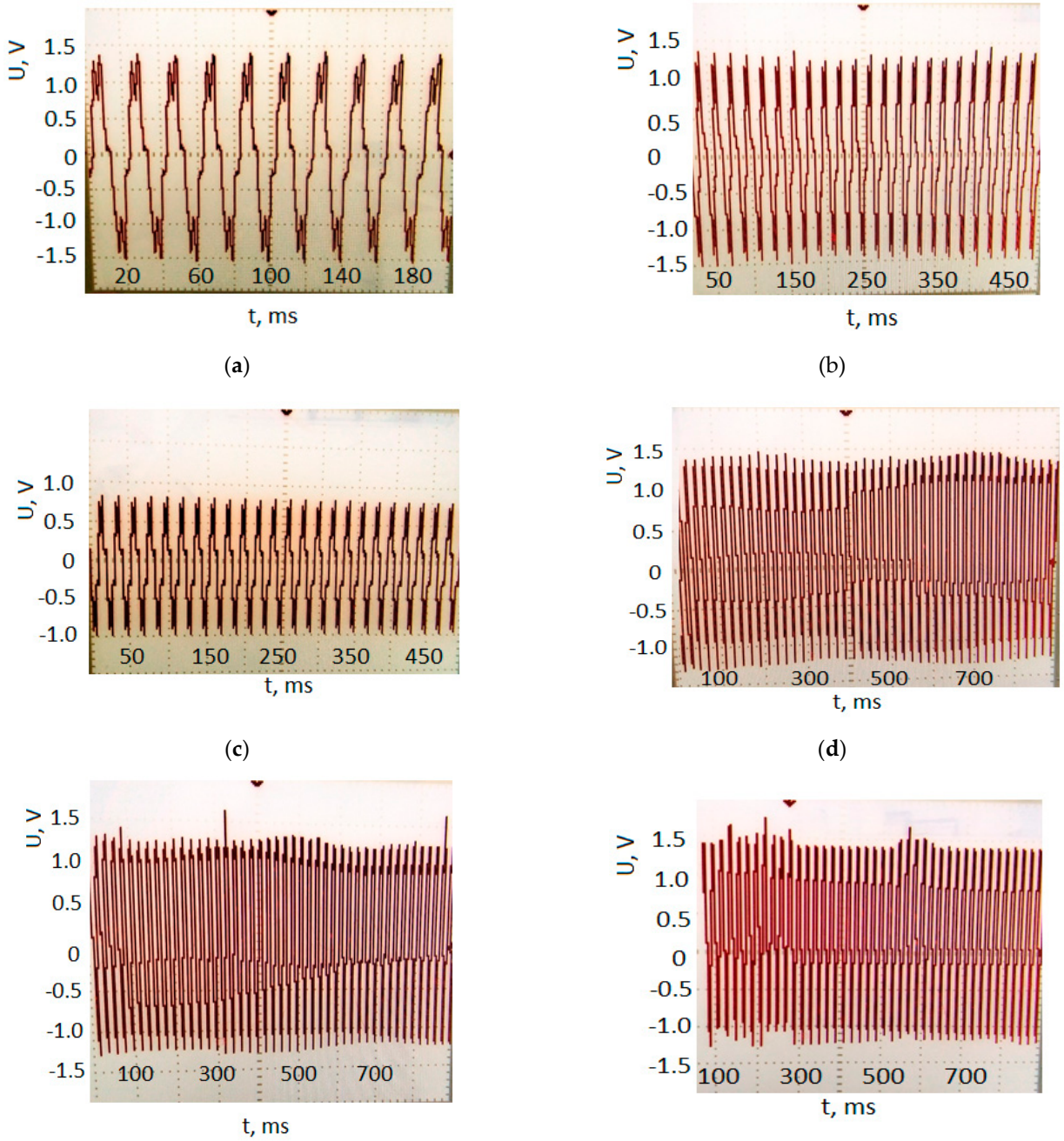

Figure 6. Oscillograms of the output voltage of the flexible piezoelectric transducers with BST only and hybrid BST+PVDF-TrFE films at different duration of bending: BST at switching (**a**); BST after 1 h of bending (**b**); BST after 2 h of bending (**c**); hybrid BST+PVDF-TrFE at switching (**d**); hybrid BST+PVDF-TrFE after 1 h of bending (**e**); hybrid BST+PVDF-TrFE after 2 h of bending (**f**).

Table 2. Summarized values of the open circuit RMS voltage, short circuit current, and power produced at different durations of bending applied onto the BST and hybrid BST+PVDF-TrFE sample.

Parameter	At Switching			After 1 h			After 2 h		
	U_{rms}, mV	I_{sc}, μA	P_o, μW	U_{rms}, mV	I_{sc}, μA	P_o, μW	U_{rms}, mV	I_{sc}, μA	P_o, μW
BST only sample	334.8	0.7	0.23	313.9	0.4	0.12	97.2	0.1	0.09
BST+PVDF-TrFE hybrid sample	323	2.3	0.74	315.4	2.11	0.66	313.5	1.97	0.61

As can be seen from Table 2 and Figure 7, comparing the RMS values of the output voltages at different bending durations, the initial output voltage was similar for the two kind of samples; however, the current through the hybrid device was three times higher due to the lower impedance and greater contact area of the smoother film at the electrode interfaces. As a result, the produced power without load was more than three times higher, as compared to the single materials BST-based transducer. A second consequence of the hybrid structure and insertion of piezoelectric polymeric films was the achieved better stability of the electrical parameters against long-term bending.

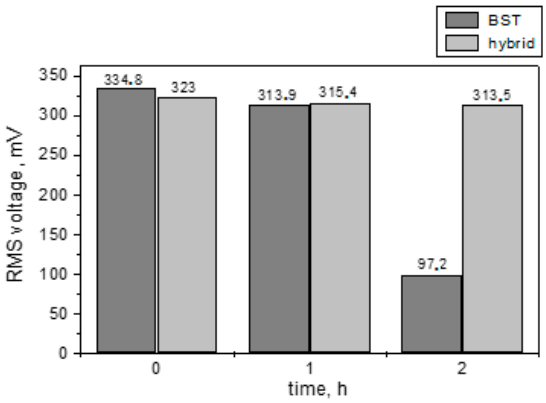

Figure 7. Degradation of the output RMS voltage for the BST and hybrid BST+PVDF-TrFE piezoelectric thin-film flexible transducers.

The RMS voltage for the BST sample decreased by 6% after one hour of bending and dropped sharply to 70.1% after 2 h due to degradation of the film and probably degradation of the interfaces [37]. On the contrary, the hybrid device exhibited stable electrical behavior against the time, which is evidence of the reinforced strength of the sample due to the insertion of the piezoelectric polymer with low Young modulus, partially absorbing the intensity of the mechanical loading in such an extent to avoid BST film degradation, and at the same time, to keep the output voltage and current competitive to the BST-only device. The relative instability of the RMS voltage for the hybrid device was 2.3% after one hour of bending and remained almost unchanged after 2 h, namely 2.9%, which is not significant degradation.

A table for comparison of different hybrid biomaterial devices produced by the microfabrication technology is shown in Table 3. In most of the papers, the durability was not discussed, or the number of bending cycle was not shown. However, the electrical parameters against the films' thicknesses are interesting to compare.

Table 3. A comparative table for the main electrical parameters, considering the thickness of the incorporated piezoelectric film or composite.

Reference	Composition	U_o, mV	I_{sc}, μA	Geometrical Parameters	Durability
[26]	$BaTi_{(1-x)}Zr_xO_3$(BTZO)/PVDF	1190 @ 21 Hz	1.35	200 nm	N/A
[38]	$BaTO_3$PVDF-HFP	14	4	200 nm	N/A
[27]	KNN/PVDF	18	2.6	105 nm	N/A
[39]	NiO@ SiO_2 (15 wt%)/PVDF	53	0.3	<100 nm	N/A
This work	$Ba_{0.5}Sr_{0.5}TO_3$/PVDF-TrFE	433 @ 48 Hz	2.3	815 nm	345,600 bends

4. Conclusions

Today, the world is surrounded by smart wireless devices that require a sustainable and ecological source of energy. Piezoelectric flexible generators are quickly emerging as highly efficient, cost-effective, and easy-to-produce power sources. The novel piezoelectric material systems and device architectures can support the development of flexible, self-powered, multifunctional electronics for human motion velocity detection, as well

as various implantable devices that do not require external power supply for biomedical energy harvesting, health monitoring, independent temperature monitoring, and pressure control, which can be built based on a piezoelectric hybrid device, consisting of oxide and polymer. It was found that a system based on BST, giving a relatively high yield in composite mixture with PVDF-TrFE, which is a possible approach to reinforce the resistance of the piezoelectric transducers against degradation, has not been studied.

Considering that the energy conversion efficiency of pure polymer materials is quite low, which prevents their use as mechanical-to-electrical transducers, its insertion as a piezoelectric active secondary phase to create organic/inorganic composites is a promising strategy for the design of new piezoelectric materials. In this context, PVDF and its copolymers would be suitable host materials for the guest oxides, having high piezoelectric constant. The spray deposition technique was used for the deposition of the polymeric film, which resulted in smooth and uniform films improving the interfacial conditions for charge transfer. In the course of the research, an innovative approach was developed, which allows the fabrication of energy harvesting hybrid element based on an unexplored composite between $Ba_{0.5}Sr_{0.5}TO_3$ and PVDF-TrFE.

It was demonstrated that although the composite structure exhibited approximately 12 mV lower piezoelectric voltage, as compared to the BST one, the polarization current was three times higher, which resulted in a triple enhancement of the produced output power. The piezoelectric module was found to be seven percent higher for the BST+PVDF-TrFE sample and the relative instability of the RMS voltage for the hybrid device was almost unchanged with the duration of the applied dynamic load, namely 2.9% after 345,600 bending cycles. The durability of the hybrid device was more than three times better than the device non-containing piezoelectric polymer. The system can capture energy from everyday human activity, exhibiting sufficient yield, according to the state-of-the-art for thin-film wearable transducers, and demonstrated higher piezoelectric response as compared to the pure BST-only, or PVDF-only single material device. At the same time, the stability of the response was maintained close to 97%, which indicated the excellent durability of the hybrid device. Thus, the results of the experiments provide a good basis for the development of electric wearable and self-powered systems such as a step forward in the design of lead-free, low-cost sustainable systems. Therefore, future work will be related to study the effect of electrical load on the device's performance, a cross-sectional observation of the contact between the layers by a scanning electron microscopy and beta sheets calculations, along with piezoelectric response of PVDF-only case.

Author Contributions: Conceptualization, M.A., K.N. and I.K.; methodology, M.A. and K.N.; software, M.A. and L.T.; validation, M.A., L.T. and K.N.; formal analysis, M.A. and K.N.; investigation, M.A. and L.T.; resources, I.K.; data curation, K.N.; writing—original draft preparation, M.A.; writing—review and editing, K.N. and I.K.; visualization, M.A. and L.T.; supervision, K.N. and I.K.; project administration, I.K.; funding acquisition, I.K. All authors have read and agreed to the published version of the manuscript.

Funding: This research was funded by the European Regional Development Fund within the Operational Programme "Science and Education for Smart Growth 2014–2020" under the Project CoE "National center of mechatronics and clean technologies" BG05M2OP001-1.001-0008, 2018–2023. The APC was funded by the same project.

Institutional Review Board Statement: Not applicable.

Informed Consent Statement: Not applicable.

Data Availability Statement: The data presented in this study are available on request from the corresponding author.

Acknowledgments: The authors acknowledge Velitchka Strizhkova from IOMT, BAS for the AFM images.

Conflicts of Interest: The authors declare no conflict of interest.

References

1. Yazid, E.; Nugraha, A.S. Energy Harvesting from a Crane System by a Piezoelectric Energy Harvester: Two Concentrated Moving Masses Approach. *Int. J. Mech. Eng. Robot. Res.* **2019**, *8*, 940. [CrossRef]
2. Liu, H.; Zhong, J.; Lee, C.; Lee, S.-W.; Lin, L. A comprehensive review on piezoelectric energy harvesting technology: Materials, mechanisms, and applications. *Appl. Phys. Rev.* **2018**, *5*, 041306. [CrossRef]
3. Safaei, M.; Sodano, H.; Anton, S. A review of energy harvesting using piezoelectric materials: State-of-the-art a decade later (2008–2018). *Smart Mater. Struct.* **2019**, *28*, 113001. [CrossRef]
4. Surmenev, R.A.; Orlova, T.; Chernozem, R.V.; Ivanova, A.A.; Surmeneva, M.A. Hybrid lead-free polymer-based nanocomposites with improved piezoelectric response for biomedical energy-harvesting applications: A review. *Nano Energy* **2019**, *62*, 475. [CrossRef]
5. Ponnamma, D.; Parangusan, H.; Tanvir, A.; AlMa'adeed, M.A.A. Smart and robust electrospun fabrics of piezoelectric polymer nanocomposite for self-powering electronic textiles. *Mater. Des.* **2019**, *184*, 108176. [CrossRef]
6. Jin, W.; Wang, Z.; Huang, H.; Hu, X.; He, Y.; Li, M.; Li, L.; Gao, Y.; Hu, Y.; Gu, H. High-performance piezoelectric energy harvesting of vertically aligned Pb(Zr,Ti)O_3 nanorod arrays. *RSC Adv.* **2018**, *8*, 7422–7427. [CrossRef]
7. Kang, H.B.; Han, C.S.; Pyun, J.C.; Ryu, W.H.; Kang, C.Y.; Cho, Y.S. (Na,K)NbO_3 nanoparticle-embedded piezoelectric nanofiber composites for flexible nanogenerators. *Compos. Sci. Technol.* **2015**, *111*, 1–8. [CrossRef]
8. Wei, H.; Wang, H.; Xia, Y.; Cui, D.; Shi, Y.; Dong, M.; Liu, C.; Ding, T.; Zhang, J.; Ma, Y.; et al. An overview of lead-free piezoelectric materials and devices. *J. Mater. Chem. C* **2018**, *6*, 12446–12467. [CrossRef]
9. Wu, J. Perovskite lead-free piezoelectric ceramics. *J. Appl. Phys.* **2020**, *127*, 190901. [CrossRef]
10. Barrientos, G.; Clementi, G.; Trigona, C.; Ouhabaz, M.; Gauthier-Manuel, L.; Belharet, D.; Margueron, S.; Bartasyte, A.; Malandrino, G.; Baglio, S. Lead-Free $LiNbO_3$ Thick Film MEMS Kinetic Cantilever Beam Sensor/Energy Harvester. *Sensors* **2022**, *22*, 559. [CrossRef]
11. Wlazło, M.; Haras, M.; Kołodziej, G.; Szawcow, O.; Ostapko, J.; Andrysiewicz, W.; Kharytonau, D.S.; Skotnicki, T. Piezoelectric Response and Substrate Effect of ZnO Nanowires for Mechanical Energy Harvesting in Internet-of-Things Applications. *Materials* **2022**, *15*, 6767. [CrossRef]
12. Serairi, L.; Leprince-Wang, Y. ZnO Nanowire-Based Piezoelectric Nanogenerator Device Performance Tests. *Crystals* **2022**, *12*, 1023. [CrossRef]
13. Clementi, G.; Cottone, F.; Di Michele, A.; Gammaitoni, L.; Mattarelli, M.; Perna, G.; López-Suárez, M.; Baglio, S.; Trigona, C.; Neri, I. Review on Innovative Piezoelectric Materials for Mechanical Energy Harvesting. *Energies* **2022**, *15*, 6227. [CrossRef]
14. Chen, X.; Tian, H.; Li, X.; Shao, J.; Ding, Y.; An, N.; Zhoua, Y. A high performance P(VDF TrFE) nanogenerator with self-connected and vertically integrated fibers by patterned EHD pulling. *Nanoscale* **2015**, *7*, 11536–11544. [CrossRef]
15. Wu, L.; Jin, Z.; Liu, Y.; Ning, H.; Liu, X.; Alamusi; Hu, N. Recent advances in the preparation of PVDF-based piezoelectric materials. *Nanotechnol. Rev.* **2022**, *11*, 1386–1407. [CrossRef]
16. Mahmoodi, S.; Hamedi, P.; Zhong, S.; Weidner, D.; Li, W. Compressibility and crystalline structures of PVDF membranes under elevated gravity acceleration by two-axis spin coating technology. *Phys. Chem. Chem. Phys.* **2022**, *24*, 17577–17592. [CrossRef]
17. Li, Y.; Hu, Q.; Zhang, R.; Ma, W.; Pan, S.; Zhao, Y.; Wang, Q.; Fang, P. Piezoelectric Nanogenerator Based on Electrospinning PVDF/Cellulose Acetate Composite Membranes for Energy Harvesting. *Materials* **2022**, *15*, 7026. [CrossRef] [PubMed]
18. He, Z.; Rault, F.; Vishwakarma, A.; Mohsenzadeh, E.; Salaün, F. High-Aligned PVDF Nanofibers with a High Electroactive Phase Prepared by Systematically Optimizing the Solution Property and Process Parameters of Electrospinning. *Coatings* **2022**, *12*, 1310. [CrossRef]
19. Wan, C.; Bowen, C.R. Multiscale-structuring of polyvinylidene fluoride for energy harvesting: The impact of molecular-, micro- and macro-structure. *J. Mater. Chem. A* **2017**, *5*, 3091–3128. [CrossRef]
20. Sriphan, S.; Vittayakorn, N. Hybrid piezoelectric-triboelectric nanogenerators for flexible electronics: Recent advances and perspectives. *J. Sci. Adv. Mater. Devices* **2022**, *7*, 100461. [CrossRef]
21. Zhang, T.; Yang, T.; Zhang, M.; Bowen, C.R.; Yang, Y. Recent Progress in Hybridized Nanogenerators for Energy Scavenging. *Iscience* **2020**, *23*, 101689. [CrossRef]
22. Sriphan, S.; Charoonsuk, T.; Maluangnont, T.; Vittayakorn, N. High-performance hybridized composited-based piezoelectric and triboelectric nanogenerators based on $BaTiO_3$/PDMS composite film modified with $Ti_{0.8}O_2$ nanosheets and silver nanopowders cofillers. *ACS Appl. Energy Mater.* **2019**, *2*, 3840–3850. [CrossRef]
23. Sajad Sorayani Bafqi, M.; Bagherzadeh, R.; Latifi, M. Fabrication of composite PVDF-ZnO nanofiber mats by electrospinning for energy scavenging application with enhanced efficiency. *J. Polym. Res.* **2015**, *22*, 130. [CrossRef]
24. Kim, Y.W.; Lee, H.B.; Yeon, S.M.; Park, J.H.; Lee, H.J.; Yoon, J.; Park, S.H. Enhanced Piezoelectricity in a Robust and Harmonious Multilayer Assembly of Electrospun Nanofiber Mats and Microbead-Based Electrodes. *ACS Appl. Mater. Interfaces* **2018**, *10*, 5723–5730. [CrossRef] [PubMed]
25. Jeong, C.K.; Baek, C.; Kingon, A.I.; Park, K.; Kim, S.-H. Lead-Free Perovskite Nanowire-Employed Piezopolymer for Highly Efficient Flexible Nanocomposite Energy Harvester. *Small* **2018**, *14*, e1704022. [CrossRef] [PubMed]
26. Genchi, G.G.; Ceseracciu, L.; Marino, A.; Labardi, M.; Marras, S.; Pignatelli, F.; Bruschini, L.; Mattoli, V.; Ciofani, G. P(VDF-TrFE)/$BaTiO_3$ nanoparticle composite films mediate piezoelectric stimulation and promote differentiation of SH-SY5Y neuroblastoma cells. *Adv. Healthc. Mater.* **2016**, *5*, 1808–1820. [CrossRef] [PubMed]

27. Li, C.; Wang, L.; Chen, W.; Lu, L.; Nan, H.; Wang, D.; Zhang, Y.; Yang, Y.; Jia, C.L. A novel multiple interface structure with the segregation of dopants in lead-free ferroelectric $(K_{0.5}Na_{0.5})NbO_3$ thin films. *Adv. Mater. Interfaces* **2018**, *5*, 1700972. [CrossRef]
28. Nunes-Pereira, J.; Sencadas, V.; Correia, V.; Cardoso, V.F.; Han, W.; Rocha, J.G.; Lanceros-Méndez, S. Energy harvesting performance of $BaTiO_3$/poly (vinylidene fluoride–trifluoroethylene) spin coated nanocomposites. *Compos. B Eng.* **2015**, *72*, 130–136. [CrossRef]
29. Nedelchev, K.; Kralov, I. Efficiency improvement of a vibration energy harvesting generator by using additional vibrating system. *AIP Conf. Proc.* **2017**, *1910*, 020015. [CrossRef]
30. Available online: https://www.microresist.de/en/produkt/ma-p-1200-series-ma-p-1275-hv/ (accessed on 28 December 2022).
31. Aleksandrova, M.; Ivanova, T.; Koch, S.; Hamelmann, F.; Karashanova, D.; Gesheva, K. Study of Sputtered Barium Strontium Titanate Films for Energy Harvesting Applications. *Adv. Mater. Lett.* **2020**, *11*, 1–7. [CrossRef]
32. Tian, B.B.; Bai, X.F.; Liu, Y.; Gemeiner, P.; Zhao, X.L.; Liu, B.L.; Zou, Y.H.; Wang, X.D.; Huang, H.; Wang, J.L.; et al. β phase instability in poly(vinylidene fluoride/trifluoroethylene) thin films near β relaxation temperature. *Appl. Phys. Lett.* **2015**, *106*, 092902. [CrossRef]
33. Monshi, A.; Reza Foroughi, M.; Reza Monshi, M. Modified Scherrer Equation to Estimate More Accurately Nano-Crystallite Size Using XRD. *World J. Nano Sci. Eng.* **2012**, *2*, 154–160. [CrossRef]
34. Tian, G.; Deng, W.; Xiong, D.; Yang, T.; Zhang, B.; Ren, X.; Lan, B.; Zhong, S.; Jin, L.; Zhang, H.; et al. Dielectric micro-capacitance for enhancing piezoelectricity via aligning MXene sheets in composites. *Cell Rep. Phys. Sci.* **2022**, *3*, 100814. [CrossRef]
35. Nguyen, B.-P.; Tran, Q.H.; Nguyen, T.-T.; Pradhan, A.M.S.; Huynh, T.-C. Understanding Impedance Response Characteristics of a Piezoelectric-Based Smart Interface Subjected to Functional Degradations. *Complexity* **2021**, *2021*, 1–24. [CrossRef]
36. Ion, V.; Craciun, F.; Scarisoreanu, N.D.; Moldovan, A.; Andrei, A.; Birjega, R.; Ghica, C.; Di Pietrantonio, F.; Cannata, D.; Benetti, M.; et al. Impact of thickness variation on structural, dielectric and piezoelectric properties of $(Ba,Ca)(Ti,Zr)O_3$ epitaxial thin films. *Sci. Rep.* **2018**, *8*, 1–9. [CrossRef] [PubMed]
37. Salazar, R.; Larkin, K.; Abdelkefi, A. Piezoelectric property degradation and cracking impacts on the lifetime performance of energy harvesters. *Mech. Syst. Signal Process.* **2021**, *156*, 107697. [CrossRef]
38. Fu, J.; Hou, Y.; Zheng, M.; Zhu, M. Comparative study of dielectric properties of the PVDF composites filled with spherical and rod-like $BaTiO_3$ derived by molten salt synthesis method. *J. Mater. Sci.* **2018**, *53*, 7233–7248. [CrossRef]
39. Dutta, B.; Kar, E.; Bose, N.; Mukherjee, S. NiO@ SiO_2/PVDF: A Flexible Polymer Nanocomposite for a High Performance Human Body Motion-Based Energy Harvester and Tactile e-Skin Mechanosensor. *ACS Sustain. Chem. Eng.* **2018**, *6*, 10505–10516. [CrossRef]